Selected Research Projects in Experimental and Computational Photonics

Hua Tu

Reader's Guide

This document presents three research projects in **hybrid quantum systems, nonlinear photonics, and electro-optical engineering**, unified by a system-level philosophy that tightly integrates optical dynamics, electronic interfaces, and control or learning algorithms.

Part I investigates chip-scale quantum noise detection through **shot-noise-limited balanced homodyne detection for thin-film lithium niobate (TFLN) squeezing experiments**. I identified optical coupling, not electronic noise, as the dominant bottleneck and addressed it through co-designed fiber-to-chip edge couplers, free-space mode matching, wideband RF readout electronics, and common-mode rejection techniques to achieve shot-noise-limited performance.

Part II develops a **hardware-in-the-loop nonlinear photonic computing platform** based on second-harmonic generation. To enable gradient-based learning on non-differentiable optical hardware, I introduced a framework combining a noise-aware, differentiable digital twin with constraint-aware optimization. Using this approach, I demonstrated 85% accuracy on a vowel recognition task, validating end-to-end trainable nonlinear optics.

Part III addresses **state-dependent dynamic control in precision photonic systems**, using **microwave-to-optical (M2O) transduction** as a case study. I diagnosed repeated lock–unlock failures in **multi-cavity filter** chains as control-path mismatches. I combined hardware and software, enabling robust, repeatable dynamic pump filtering. This capability is essential for future single-photon-level quantum transduction.

Each part is self-contained and can read independently.

Contents

Shot-Noise-Limited Balanced Homodyne Detection for TFLN Squeezing Measurement

Opening

Achieving reliable squeezing measurements on integrated photonic platforms critically depends on operating balanced homodyne detection (BHD) at the shot-noise limit. On 300 nm **thin-film lithium niobate (TFLN)** waveguides with sub-micron mode confinement, however, I find that fiber-to-chip mode mismatch, optical loss, electronic noise, and limitations in the RF readout chain collectively prevent shot-noise-limited operation. These factors degrade the effective detection efficiency and directly suppress observable squeezing.

To address these system-level bottlenecks, I design a co-optimized homodyne detection architecture that integrates **nanophotonic coupling structures, free-space and fiber-based optical interfaces, and wideband low-noise RF readout electronics**, rather than optimizing components in isolation. By explicitly modeling how optical loss, electronic noise, and imperfect common-mode rejection translate into measurable squeezing degradation, I establish a practical pathway toward high-efficiency, quantum-limited homodyne detection for on-chip squeezing experiments.

Objective: Shot-Noise-Limited Balanced Homodyne Detection

Reliable on-chip squeezing measurements require **balanced homodyne detection (BHD) operating at the shot-noise limit**. On 300 nm thin-film lithium niobate (TFLN) platforms, however, I find that fiber-to-chip mode mismatch, optical loss, electronic noise, and imperfect common-mode rejection collectively suppress observable squeezing. To overcome these system-level bottlenecks, I co-design an integrated BHD interface spanning nanophotonic couplers, optical layouts, and wideband RF electronics. I enabled a shot-noise-limited operation with **19.6 dB clearance** and **26 dB CMRR**., 73.4% quantum efficienct. A 97% quantum efficiency module is under characterization.

Loss-Induced Squeezing Degradation

Effect of Optical Loss on Measured Squeezing
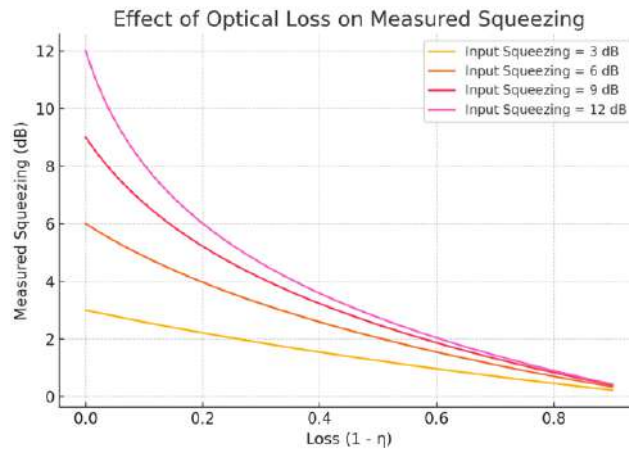
η is the overall effective detection efficiency

$$\eta = \eta_{\text{coupling}} \times \eta_{\text{QE}}$$

Optical loss mixes vacuum noise and suppresses measurable squeezing

$$< X^2_{out} > \ = \eta < X^2_s > + (1 - \eta) < X^2_{vac} >$$

$$V_{out} = \eta V_{in} + (1 - \eta)$$

1. Balanced Homodyne Detection Interface with Taper Design

1.1 Fiber Couple Detector Analysis

- **Detector Quantum Efficiency (η_{QE}):**
    - **PDB770C:** 73.4%
    - **BDXQ1F:** 97%

However, I identify chip-to-fiber coupling (η_coupling) as the dominant bottleneck limiting total detection efficiency. To address this, I design an **edge-lens coupler for our 300 nm TFLN waveguide**, achieving **65% coupling efficiency** to a lensed fiber with 2.5 μm mode diameter (product of transmission and mode overlap).
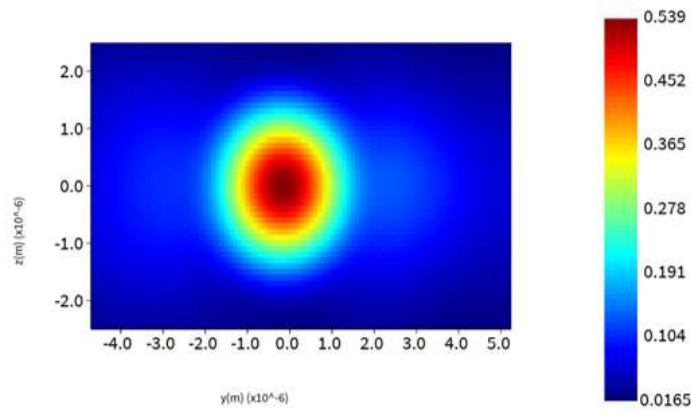
2. Free Space Detection Analysis

I also explore free-space coupling as an alternative interface. The small vertical mode size of the 300 nm TFLN waveguide limits collection efficiency with standard optics (NA = 0.85). In comparison, a 500 nm platform supports a larger mode and achieves 70% coupling (reported in literature), while the 300 nm device yields only ~49%.*

Waveguide Structure	300 nm Waveguide	500 nm Waveguide
Rib Height	120 nm	300 nm
Slab Height	180 nm	200 nm
Lens NA	0.85	0.85
Coupling Efficiency	49%	70% (reported in the paper)

$$\eta_x = 1 - exp(-2 \times (\frac{tan(\theta_{lens})}{tan(\theta_{beam,x})})^2) \approx 49\%$$

Free Space BHD Optical Layout

To improve this, I design tapers that expand the mode diameter beyond 1 µm (current simulation target: 2.5 µm). If fabricated successfully, such modes would enable >90% free-space coupling.

For the current setup, I optimize the optical layout to minimize loss:
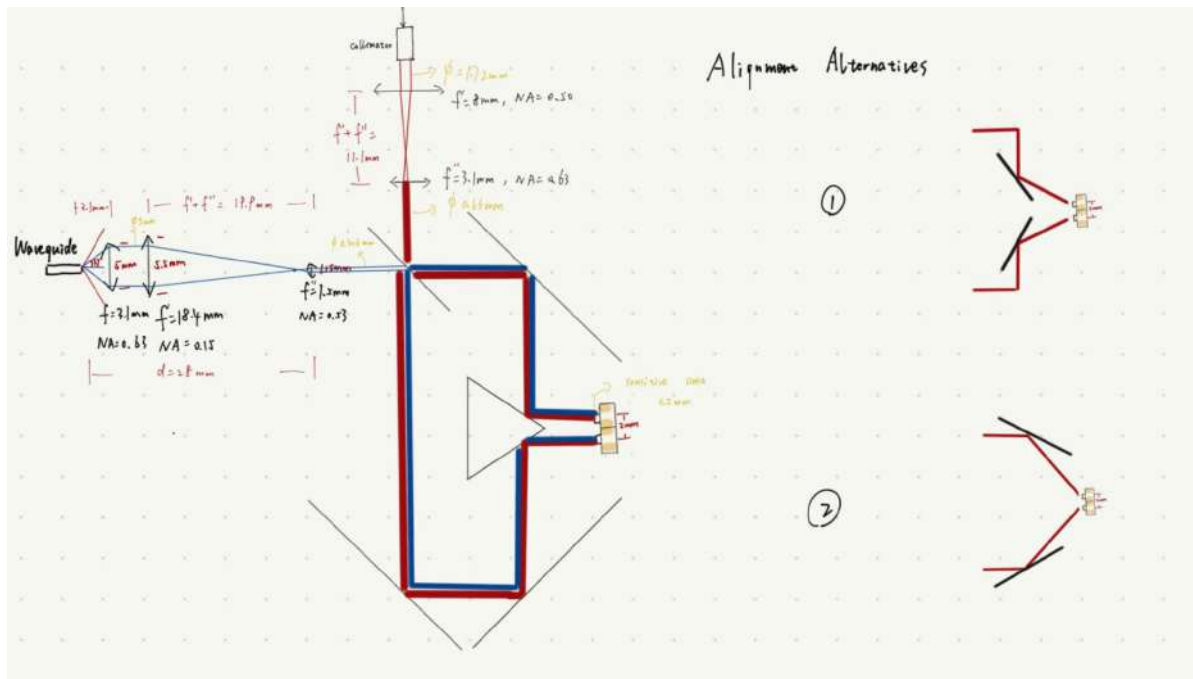
- **Squeezed Light:** Collimated to 5 mm diameter, then reduced via $4f$ system to 0.416 mm.
- **LO Light:** Collimated to 1.72 mm, reduced to 0.66 mm to fully cover the signal beam.
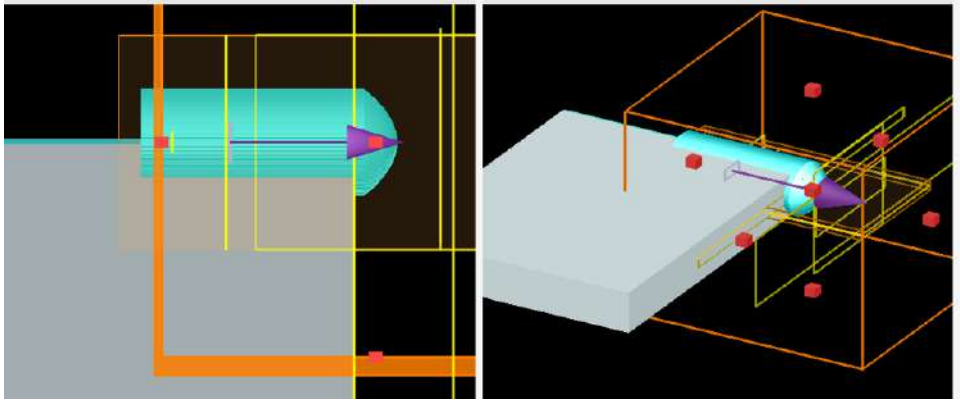
By combining this layout with high-QE photodiodes, I project a **total detection efficiency exceeding 80%** for the free-space interface..**

I have also **developed the PCB Layout in KiCad** to support the impedance matching.
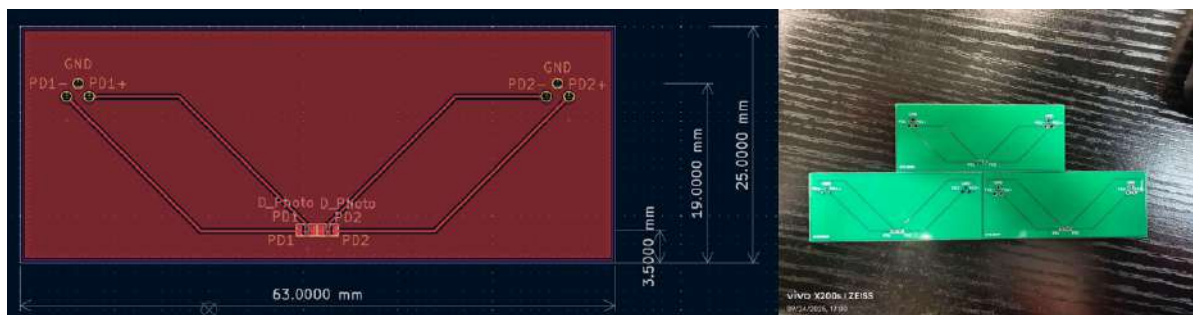
2. Fiber-to-Chip Coupling: Edge Coupler Modeling and Optimization

2.1 Edge-Lens Coupler Design on 300 nm LN waveguide (no slab)

I designed lens coupler (refractive index = 1.63): written on top of the TFLN waveguide facet

Custom even-order aspheric edge-lens: geometry is defined by an even-order radial polynomial, up to the fourth order

$$h(r) = c_0 + c_2 \cdot 10^3 \cdot r^2 + c_4 \cdot 10^9 \cdot r^4$$

**Geometric parameters**: lens curvature, radius, axial offset

Coupling target: Lensed fiber with Gaussian mode Mode size: 2.5 μm diameter, $1/e^2$

2.2 Mode Overlap Calculation with Mode Center Bias

- Due to typical offset of the mode from the geometric center, I compute the actual waveguide mode center using custom code
- A Gaussian fiber mode (2.5 μm diameter, 1/e²) is then centered at this position to compute the accurate mode overlap.

2.3 Elliptical Asphere Design on 300 nm Squeezing LN Waveguide (120 nm slab)

Due to lateral mode expansion from rib width reduction, circular lenses cannot simultaneously optimize beam shaping in both transverse directions.
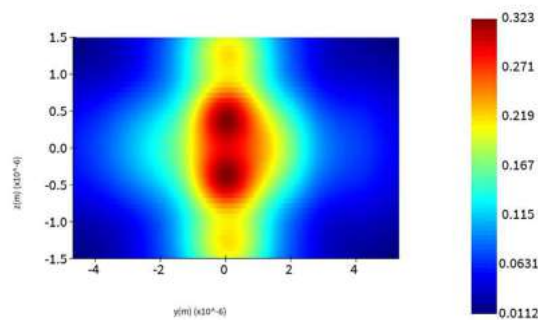
To resolve this, I design an **elliptical aspheric edge-lens**, enabling independent control over x and y divergence. My optimization targets maximum effective coupling efficiency:

FreeCAD fabrication layout
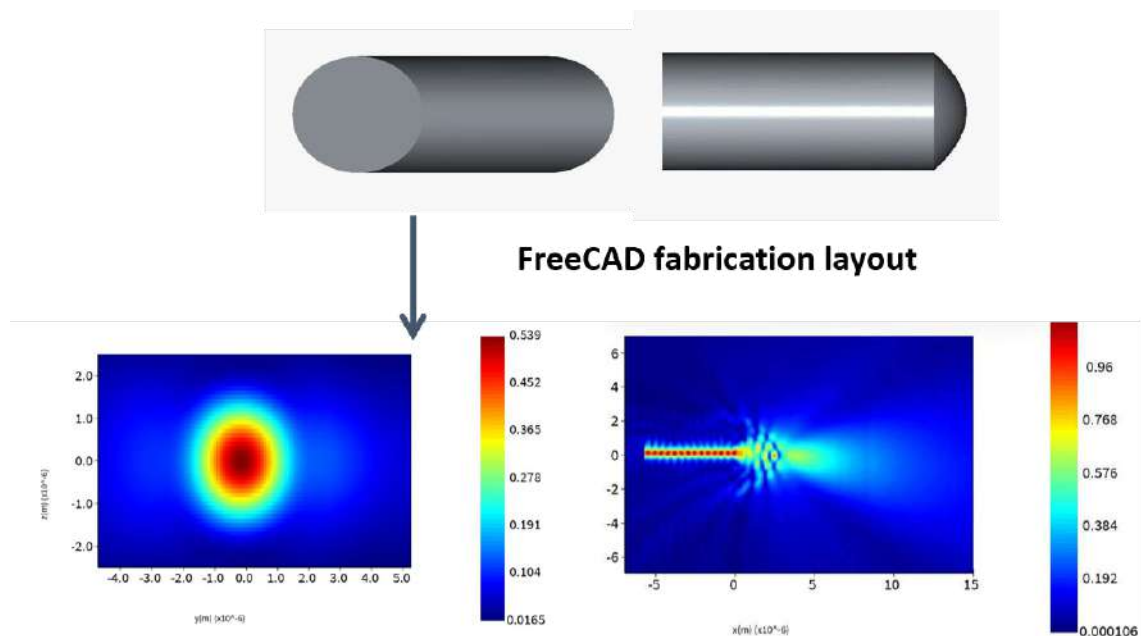
Target: maximized effective coupling efficiency

$$\eta_{total} = \eta_{geom} \times \eta_{overlap}$$

η_{geom}: geometrical transmission

$\eta_{overlap}$: mode-overlap efficiency

Through optimization, I achieved **a total coupling loss of 1.8 dB per facet** for rib TFLN waveguide.

3. Wideband RF Balanced Detector Assembly and Shot-Noise Characterization

3.1 Results Summary

Parameter	Characterization Result
Shot Noise Clearance Ratio	19.61 dB @ 10 dBm
Responsivity	0.917 A/W (Data Sheet Curve: 0.89 A/W)
Quantum Efficiency from Measured Responsivity	73.4%
CMRR	26.36 dB
NEP (RF Electronic Noise Floor)	8.6 pW/$\sqrt{Hz}$
Shot noise linear fit R^2	0.9967
Monitor Balance	below 0.2% difference
Monitor Offset	0-1mV

3.2 Low Inductance Electronic Interface for PDB770C & BDXQ1F

3.2.1 Thermal management + Electrostatic Discharge (ESD) protection

I limited **solder contact to <4 s**, and allowed **>10 s of cooling time** between joints.

3.2.2 Millimeter-scale castellated edge pads micro-soldering.
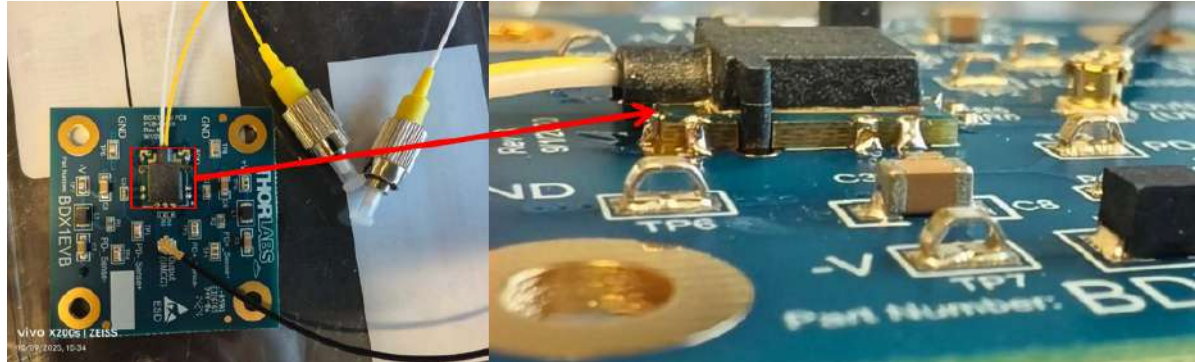
3.3 Power-On characterization

Noise Equivalent Power (NEP) - RF noise floor:

$$\text{NEP} \approx 8.57 \times 10^{-12} \ \text{W}/\sqrt{\text{Hz}}$$

$$Minimum \ \text{NEP} \ from \ spec \ sheet = 8 \times 10^{-12} \ \text{W}/\sqrt{\text{Hz}} \ (DC \ - \ 100 \ MHz))$$

This result validates the effective suppression of the electronic dark noise floor ($\text{NEP} \approx 8.57 \ \text{pW}/\sqrt{\text{Hz}}$). The shot noise is the dominant contribution to the signal.

Shot Noise Limit (SNL) and System Efficiency

All of the input power were measured by an optical power meter.
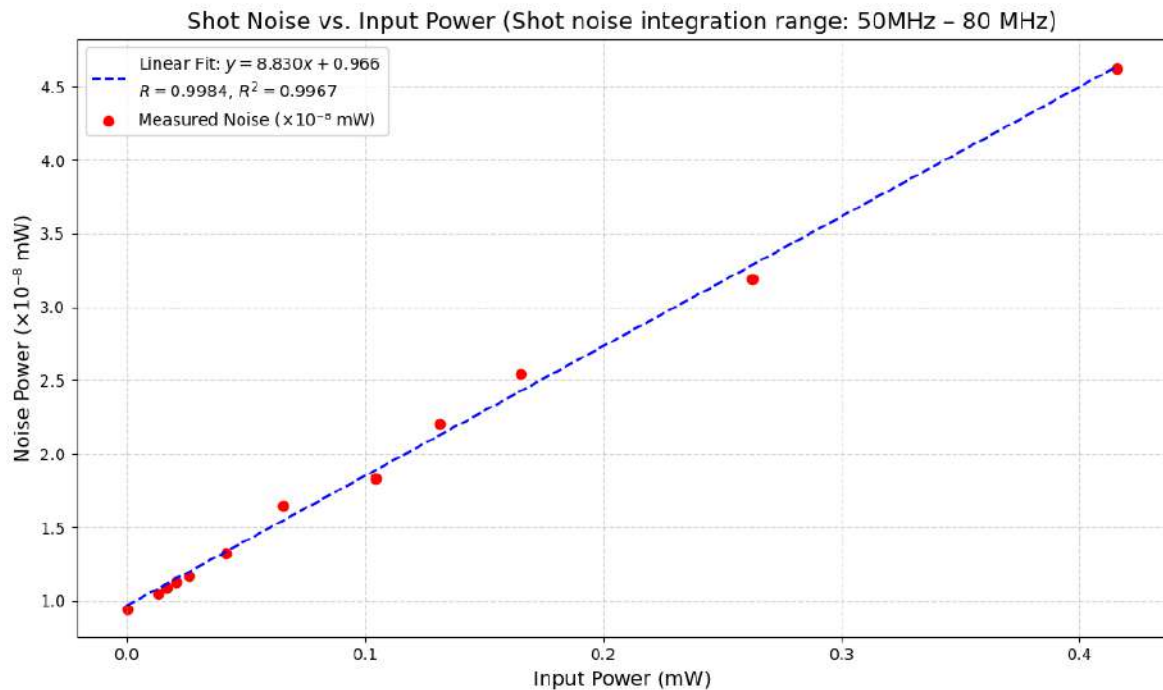
Under illumination, the RF noise scales linearly with optical power (R^2 = 0.9967), confirming shot-noise-limited operation. From the responsivity (**0.917 A/W**), I extract an effective quantum efficiency of **73.4%**. These results confirms operation deep in the **shot-noise-limited regime.**

4. Common mode rejection ratio (CMRR)

Local oscillator intensity noise (RIN) generates excess current noise $S_I^{\text{excess}} = RIN \times I^2$. In an ideal balanced homodyne detection (BHD) setup, differential detection cancels this common-mode noise. However, due to finite common-mode rejection ratio (CMRR), a residual component remains. I measure a **CMRR of 26.36 dB** (linear ratio ≈ 433), sufficient to suppress RIN below the shot-noise floor.

$$\text{CMRR}_{\text{linear}} = \frac{\text{Input Common Mode Noise } (S_I^{\text{excess}})}{\text{Residual Differential Output Noise } (S_I^{\text{excess, residual}})} \approx 433$$

$$\text{CMRR (dB)} = 10 \cdot \log_{10}(433) \approx 26.36 \text{ dB}$$

CMRR Conclusion

This result demonstrates that the system's **common-mode noise is** effectively suppressed, leaving minimal residual excess noise in the **differential** RF **signal**, and the system performance is fundamentally limited by **quantum shot noise**.

Conclusion and Outlook

In this work, I demonstrate a shot-noise-limited balanced homodyne detection platform tailored to thin-film lithium niobate squeezing experiments. I identify optical coupling loss, not photodiode quantum efficiency, as the dominant limitation on overall detection efficiency. Guided by this insight, I design and optimize inverse tapers and aspheric edge-lens couplers using full 3D electromagnetic simulations, achieving **1.8 dB per-facet coupling loss** and establishing a clear path toward further improvement.

On the detection side, I implement a wideband, low-noise RF readout chain, achieving **19.6 dB shot-noise clearance**, **73.4% effective quantum efficiency**, and **26.4 dB common-mode rejection**. The linear dependence of noise on optical power (R² = 0.9967) confirms operation deep in the shot-noise-limited regime, and the close agreement with theory validates both modeling and implementation.

Together, these results prove that **quantum-limited homodyne detection on sub-micron TFLN platforms is achievable** through coordinated co-design of photonic interfaces, optical layouts, and RF electronics. The methodologies I develop—particularly coupling-aware efficiency analysis and integrated opto-electronic optimization—are directly extensible to next-generation on-chip squeezing sources and quantum transduction experiments, where maximizing detection efficiency is essential for observing nonclassical states.

Hardware-in-the-Loop Nonlinear Photonic Computing via Noise-Aware Digital Twins and Lagrangian Optimization

Hua Tu

1. Abstract

Nonlinear optical systems offer a compelling physical substrate for analog computing due to their intrinsic ultrafast and non-Gaussian responses. However, training such hardware directly remains challenging because real optical processes are non-differentiable, noisy, and constrained by physical limits. In this work, we present a **hardware-in-the-loop nonlinear photonic computing framework** based on **second-harmonic generation (SHG)**, enabled by a **differentiable noise-aware digital twin** and **constrained optimization**.

I independently developed a first-principles SHG forward model with a learned differentiable surrogate that captures both deterministic nonlinear responses and device-specific variations. This digital twin is integrated into a **Physics-Aware Training (PAT)** pipeline, where forward propagation is performed on real hardware while gradients are computed through the surrogate model. To ensure physically valid actuation, we incorporate **Lagrangian constraints** that explicitly enforce hardware-safe bounds during optimization.

Using this hybrid framework, we demonstrate end-to-end trainable nonlinear photonic computation on a vowel recognition task, achieving **85% classification accuracy**. Our results show that nonlinear photonic hardware can be treated as a programmable computational layer when combined with differentiable modeling and constraint-aware training. This approach provides a general pathway for optimizing non-differentiable photonic systems and extends naturally to other nonlinear and quantum optical platforms.

2. System Architecture

2.1 Input Encoding: Spectral Amplitude Modulation via DMD

Input data are encoded as **spectral amplitude vectors** rather than spatial patterns. Each input specifies amplitude weights over a predefined wavelength grid, which are mapped onto a **binary digital micromirror device (DMD)** through wavelength-to-space dispersion. Individual micromirrors thus modulate distinct spectral components.

This spectral encoding provides a stable interface between numerical data and nonlinear optical hardware, while avoiding sensitivity to spatial mode variations.

2.2 First-Principles Second-Harmonic Generation Modeling and Dataset Generation

The spectrally shaped fundamental light is injected into a nonlinear medium, where **second-harmonic generation** implements a fixed quadratic transformation governed by χ^2 light–matter interaction. The resulting second-harmonic spectrum depends nonlinearly on the input amplitudes and constitutes the physical forward mapping for a neural network framework.

A **first-principles SHG based on coupled-wave equations is developed in this study** as a **physics-informed baseline**. Experimentally measured input–output pairs are collected across the operating parameter space and serve as training data for a digital surrogate that reflects real hardware behavior.

2.3 Noise-Aware Digital Twin Training for Backpropagation

Because the physical SHG process is non-differentiable and noisy, direct backpropagation through hardware is infeasible. To address this, we train a **noise-aware digital twin** on experimentally acquired SHG datasets. The digital twin captures both the deterministic nonlinear response and stochastic hardware-induced deviations.

Once trained, the digital twin is used exclusively in the **backward pass** to provide surrogate gradients for optimization.

2.4 Physics-Aware Training (PAT) Combining SHG Forward and Digital Twin Backpropagation

Figure 1. Physics-Aware Training (PAT) strategy, where forward propagation is executed on the five-layer physical SHG and gradients are computed through the digital twin.
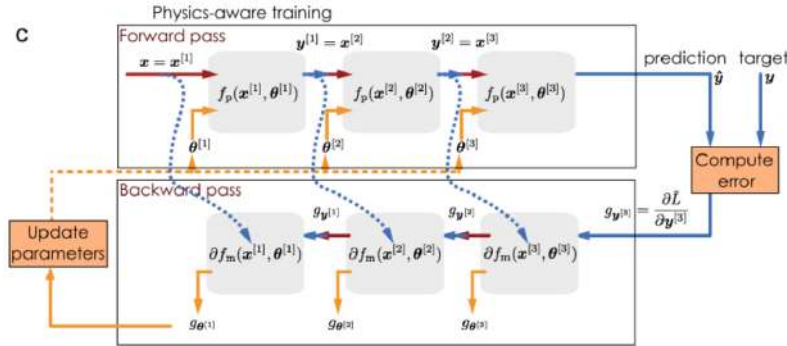
This hybrid scheme preserves fidelity to real hardware dynamics while enabling efficient gradient-based learning. Optimization is performed under explicit constraints to enforce physically valid actuation.

II. Experimental Workflow

The experimental workflow is organized into modular stages covering optical encoding, SHG spectral acquisition, digital-twin training, and physics-aware optimization. Implementation details are omitted to emphasize system-level methodology.

Input patterns are applied to a DMD through **wavelength-to-space dispersion,** and the resulting SHG spectra are measured using a calibrated spectrometer. The raw 2D spectral images are reduced to 1D spectra and further compressed to fixed-dimensional outputs for learning.

Measured **SHG spectra** are normalized and compressed from **448 dimensions to a 50-dimensional representation** via interpolation and averaging, enabling efficient downstream learning while preserving spectral structure.

Experimental control and data acquisition are implemented via a custom **Python-GPIB** interface; implementation details are omitted for clarity.

Wavelength-to-pixel mappings for both the DMD and spectrometer are obtained through **prior calibration** and reused throughout all experiments.

3. SHG-Based Physical Forward Model and Digital Twin Training

3.1 Physics-inspired SHG Forward Operator

To emulate the experimental second-harmonic generation (SHG) nonlinear transformation, I construct a physics-inspired forward operator in which output spectral components arise from **pairwise interactions of input spectral amplitudes**. Conceptually, this mapping follows the frequency-mixing relation

$$\frac{1}{\lambda_3} = \frac{1}{\lambda_1} + \frac{1}{\lambda_2}$$

For each discrete output channel, corresponding input pairs are identified on a predefined wavelength grid, and the output intensity is computed as the weighted sum of pairwise amplitude products.

This SHG-based forward layer serves as a **structured nonlinear operator** that captures the dominant interaction Of physical system, while remaining compatible with efficient numerical evaluation and integration into a hardware-in-the-loop neural network training.

3.2 Dataset Generation

Using identical spectral-amplitude inputs, I compare the responses of the physical SHG hardware and the SHG-inspired forward operator.

Figure 2. Comparison between the SHG hardware response and the SHG_formula forward layer under identical spectral-amplitude inputs, showing consistent nonlinear trends and overall spectral structure.
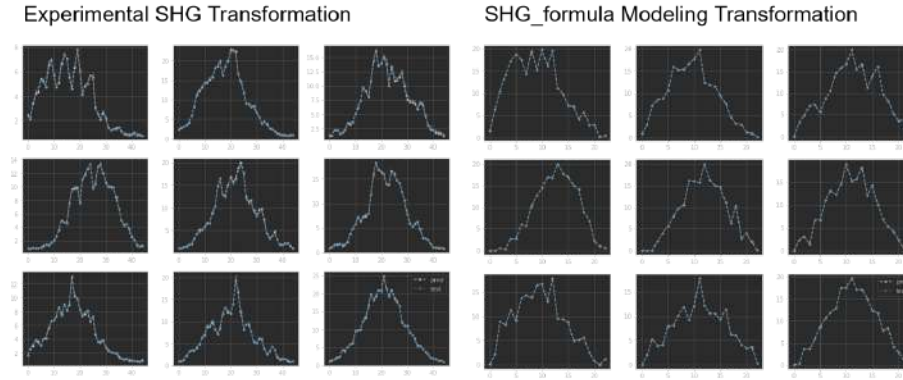
The comparison demonstrates that the forward operator reproduces the characteristic nonlinear mixing behavior observed in experiment at the level required for system-level modeling. While fine-scale spectral features differ due to experimental filtering and phase-matching effects, the overall response structure and nonlinearity are well aligned, validating the operator as a suitable abstraction for downstream learning and analysis.

The resulting paired input–output data are used to construct training datasets for the digital twin described below.

## 3.3 Noise-Aware Digital Twin Training

Why we need a differentiable noise-aware SHG model?

Direct backpropagation through the physical SHG process is infeasible due to measurement noise, hardware variability, and the absence of analytical gradients. To enable **gradient-based optimization**, I introduced a noise-aware digital twin trained on experimentally acquired SHG datasets.

The digital twin is designed to learn two complementary aspects of the hardware response:
 (i) the **deterministic nonlinear mapping** implemented by the SHG process, and
 (ii) stochastic deviations arising from **experimental noise** and device-specific fluctuations.

Figure 3. shows representative training and validation loss curves, indicating stable convergence without overfitting. Once trained, the digital twin is used **exclusively in the backward pass** to provide surrogate gradients, while all forward propagation during training is executed on the physical hardware. This separation preserves fidelity to real system dynamics while enabling efficient optimization within the Physics-Aware Training framework.
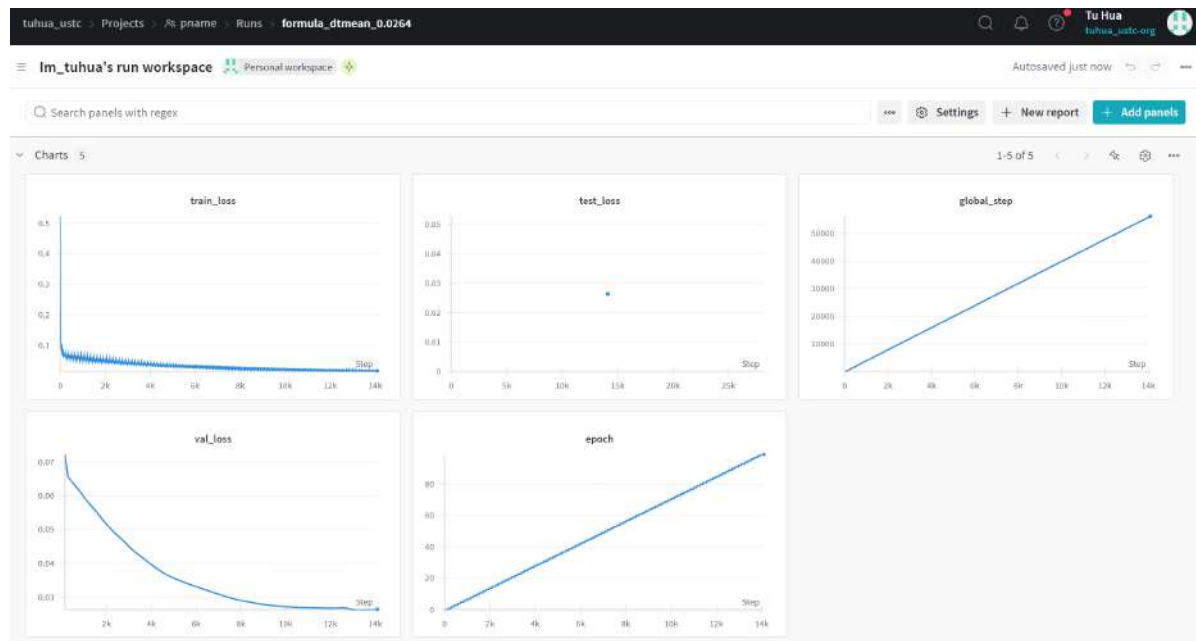
Comparison between experimentally measured SHG spectral outputs (solid lines) and digital twin predictions (dashed lines) under identical spectral-amplitude inputs. The digital twin accurately captures both the overall nonlinear spectral structure and local amplitude variations across the operating regime, providing reliable surrogate gradients for Physics-Aware Training. Minor deviations reflect stochastic measurement noise and device-specific fluctuations inherent to the physical system.

Figure 4. Digital twin fitting results for the SHG-based nonlinear transformation.
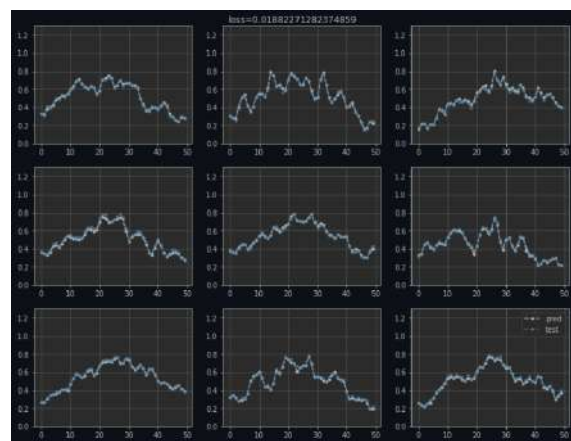
4. Constraint-Aware Optimization in Physics-Aware Training

4.1 Constraint-Aware Optimization

A central challenge in Physics-Aware Training (PAT) for nonlinear photonic hardware is enforcing **physically valid actuation during optimization**. In the SHG-based system, both input spectral amplitudes and internal learnable parameters are constrained by DMD modulation limits, optical power budgets, and nonlinear saturation. Unconstrained gradient updates can therefore drive the system into physically inaccessible or unstable regimes.

To address this, I incorporate **constraint-aware optimization** into the PAT framework using **Lagrangian penalty terms**. Instead of hard clipping, which introduces non-differentiability and disrupts gradient flow, soft penalties enforce bounded actuation while preserving smooth optimization dynamics, ensuring informative gradients near constraint boundaries.

Constraints are applied **at each SHG layer** to regulate both propagated spectral amplitudes and learnable parameters, with a **stronger penalty at the first layer** to suppress early-stage amplification and prevent error accumulation across the network.

Empirically, constraint-aware optimization is essential for stable Physics-Aware Training. Without constraints, optimization frequently diverges or converges to physically invalid solutions, even with accurate digital-twin gradients. With constraints enabled, training remains stable and converges reliably under hardware-in-the-loop settings.

4.2 Physics-Aware Training Results on Vowel Recognition

To validate the Physics-Aware Training (PAT) under physical constraints, I apply my developed digital twins and the framework to a vowel recognition task. Input samples are encoded as spectral-amplitude vectors, propagated through an SHG-based nonlinear layer, and trained end-to-end using constraint-aware optimization.

Training follows the PAT paradigm: forward propagation is executed through the SHG-based nonlinear transformation, while gradients are computed via the noise-aware digital twin.

Due to computational constraints, training is conducted for up to 600 epochs when using the SHG-based forward operator. Both training and validation losses exhibit a clear downward trend, indicating successful task learning, with moderate fluctuations attributable to the sharp spectral features of the SHG nonlinearity. Crucially, constraint-aware optimization prevents divergence and ensures convergence to physically valid solutions across repeated runs.

Figure 5. Under this training framework, the network achieves a **test accuracy of 85%** on the vowel recognition task. This result demonstrates that SHG-based optical nonlinearities, when combined with physics-aware digital twins and constraint-aware optimization, can function as effective and trainable computational layers for practical classification tasks.
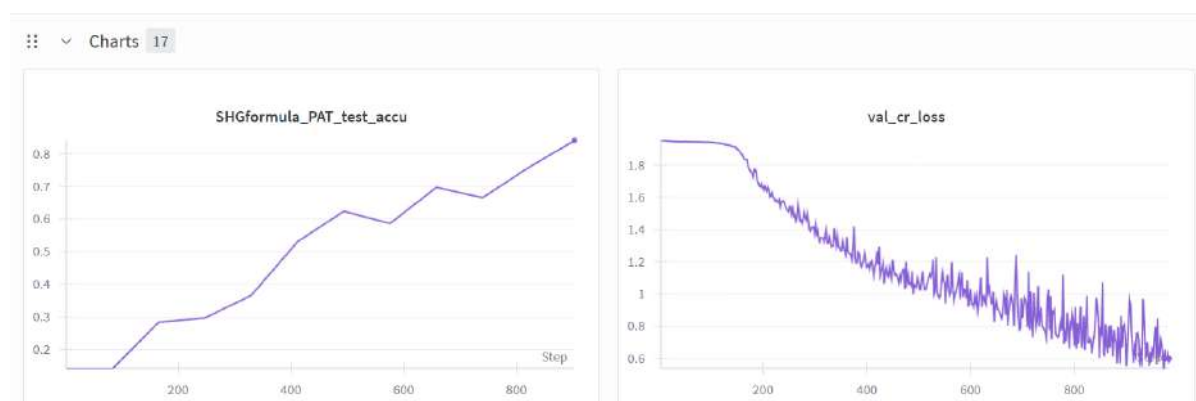
5. Conclusion

This work demonstrates that nonlinear photonic hardware, despite being non-differentiable, noisy, and physically constrained, can be **systematically trained as a programmable computational substrate** when embedded in a Physics-Aware Training framework.

By combining **hardware-in-the-loop forward propagation**, a **noise-aware differentiable digital twin**, and **constraint-aware optimization**, I establish an end-to-end training pipeline that respects physical limits while retaining the efficiency of gradient-based learning. Using second-harmonic generation (SHG) as a representative χ^2 nonlinear process, I show that experimentally measured optical nonlinearities can be abstracted into structured forward operators and paired with learned surrogates that provide reliable gradients for optimization.

Crucially, the introduction of **Lagrangian constraint enforcement** is shown to be essential for stable training. Rather than treating constraints as implementation details, this work elevates them to a core algorithmic component, ensuring physically valid actuation and preventing divergence in both hardware-in-the-loop and surrogate-based training. Under these constraints, the system achieves **85% accuracy on a vowel recognition task**, validating the feasibility of nonlinear photonic computation for practical learning problems.

Beyond the specific SHG platform, the framework presented here is **model-agnostic and extensible**. The separation of physical forward execution and differentiable backward approximation naturally generalizes to **other nonlinear and quantum optical systems where direct differentiation is impossible**. As such, this work provides a principled pathway toward training complex photonic and quantum hardware using modern learning paradigms, positioning physical dynamics not as obstacles, but as computational resources.

Robust Dynamic Laser Cleaning for Microwave-to-Optical Transduction via State-Aware Control and Hardware-Software Co-Design

## Opening: Enabling Repeatable Lock–Unlock Operation in Multi-Cavity Filter Systems

Reliable microwave-to-optical transduction measurement at the single-photon level requires stable suppression of the optical pump. This demands not only robust laser-cavity locking, but also **repeatable, low-noise transitions between locked and unlocked states** to enable background-free signal acquisition without sacrificing long-term stability.

On commercial locking platforms, however, such dynamic operation is often treated as an auxiliary feature. In **thin-linewidth, high-extinction cavity systems**, this assumption fails: during repeated lock–unlock cycles, millivolt-level offsets errors and broadband noise in **high-voltage actuation paths** convert into large effective detuning, causing loss of lock on cavity PZTs. These failures come not from inadequate feedback gain or poor PID tuning, but from the interplay between control timing, electronic noise, and the physical response of piezo-actuated cavities.

To address this, I treat the laser-cleaning stage as a **state-dependent control system**. Rather than optimizing feedback parameters in isolation, I adopt a hardware–software co-design approach that jointly considers actuation precision, noise filtering, and timing-aware control logic. This enables robust multi-cavity laser cleaning under repeated dynamic operation and achieved a **208.68uV noise RMS within 100KHz** in the lock/unlock feedback loop.

Objective:

Pump Filtering across Locking-Measurement Cycles

Single photon filtering   Pump cleaning
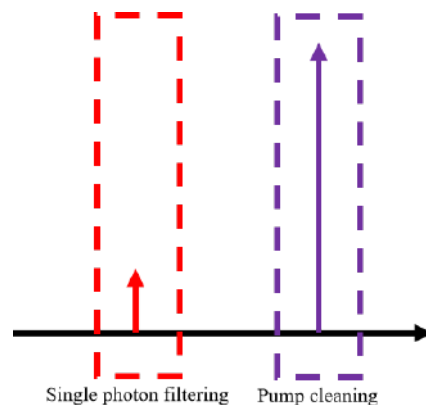
Before the detection of the signal photons, the pump should be fully filtered out.

Main challenge:

We need to **stabilize transmission in a free-running state, rather than a locked state**. Because during the free-running measurement window, feedback will contaminate the signal.

Multi-cavity pump filter bank

Pound–Drever–Hall (PDH) Locking

I implement laser–cavity stabilization using the **Pound-Drever-Hall (PDH)** technique. I apply phase modulation via an electro-optic modulator (**EOM**) and demodulate the reflected signal to generate a dispersive error signal. I feed this signal back to a piezoelectric transducer (**PZT**) controlling the cavity length, enabling robust locking with constant feedback polarity. Compared to transmission-based locking, PDH is resilient to cavity drift and well suited for the dynamic lock–unlock cycles required in laser cleaning.
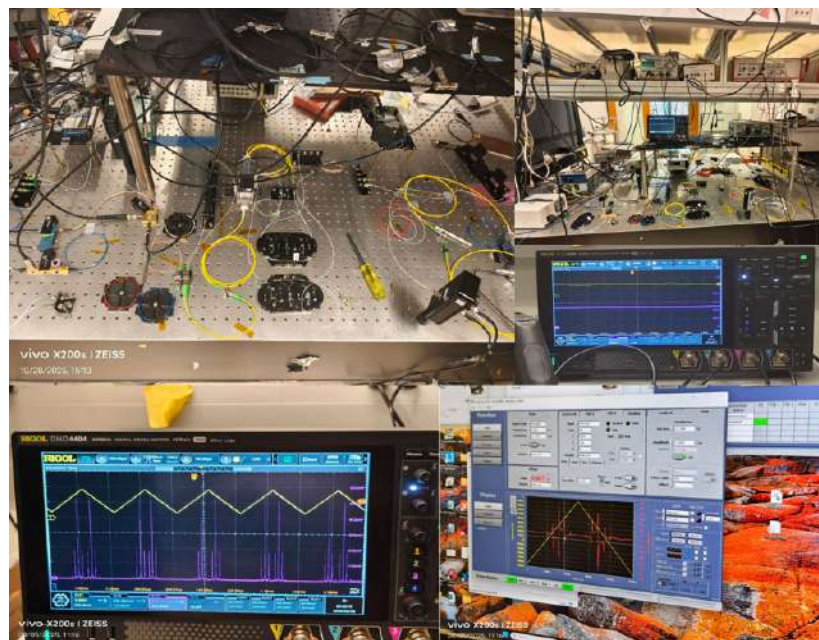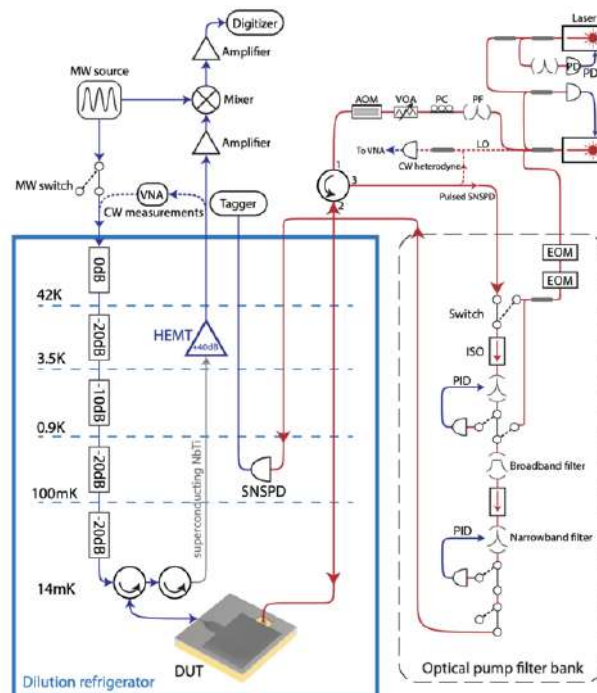
1. Control Strategy: State-Aware Locking Software Development

- Commercial controllers assume static lock
- Dynamic operation violates implicit assumptions

Using Python's telnetlib, I developed a DigiLock 110 Control Interface:

- Established 310+ full-featured DigiLock commands ()
- Unified command parser with consistent syntax
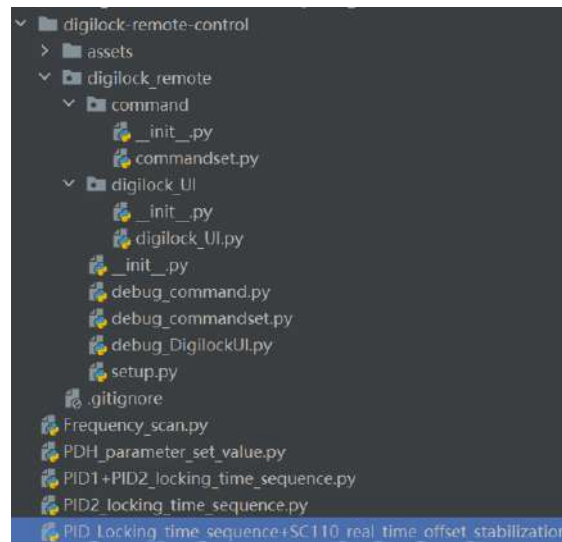

```
453    Command(name='scan:amplitude', command_type=Command_type.Numeric, queryable=True, settable=True),
454    Command(name='scan:enable', command_type=Command_type.Bool, queryable=True, settable=True),
455    Command(name='scan:frequency', command_type=Command_type.Numeric, queryable=True, settable=True),
456    Command(name='scan:output', command_type=Command_type.Enum, enum_type=Scan_output_enum, queryable=True,
457        settable=True),
458    Command(name='scan:signal type', command_type=Command_type.Enum, enum_type=Scan_waveform_enum, queryable=True,
459        settable=True),
```

Functional Modules for laser cleaning system

- PID1 + PID2 dynamic locking sequence
- PID locking time sequence with SC110 real-time offset stablization
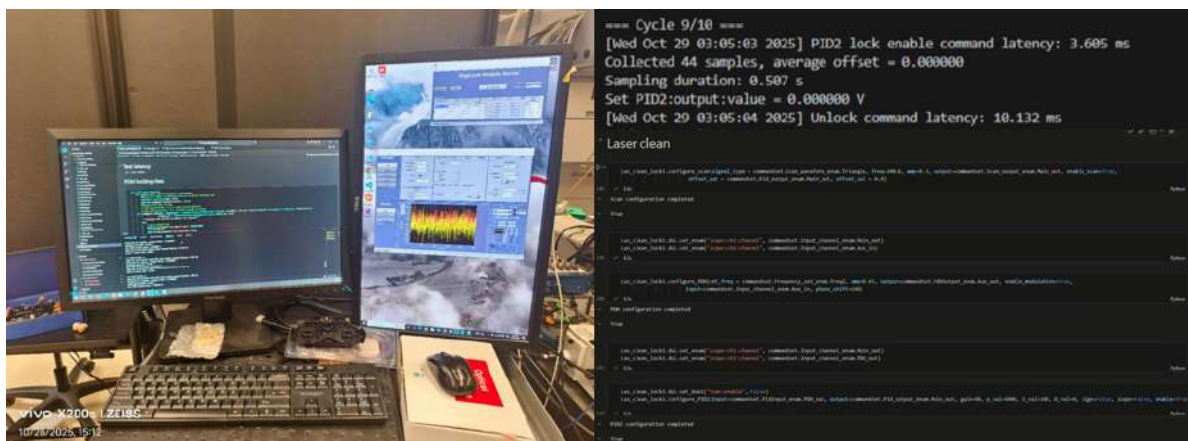- Developed a **sample-to-hold algorithm**.

```
# logic for dynamic lock–unlock control with offset holdback
enable_lock()
wait(t_lock – t_sample)

offset_avg = mean(read_offset(t_sample))
set_hold_value(offset_avg)

disable_lock()
wait(t_unlock)
```

These strategies significantly improved the lock/unlock stability.

- This strategy prevents abrupt voltage jumps that would otherwise detune the cavity. My interface runs on the lab computer with **10 ms latency**, enabling fully automated laser

cleaning. As a result, I reduce the total cleaning time from **~30 minutes to under one minute**.

2. Limitation of Commercial High-Voltage Outputs Hardware

1. A ~3 mV random error
2. Substantial output noise

The sample-to-hold routine computes the correct offset, but the SC110 outputs an incorrect voltage to the cavity PZTs, causing the cavity to **immediately fall out of lock** during the unlock phase.
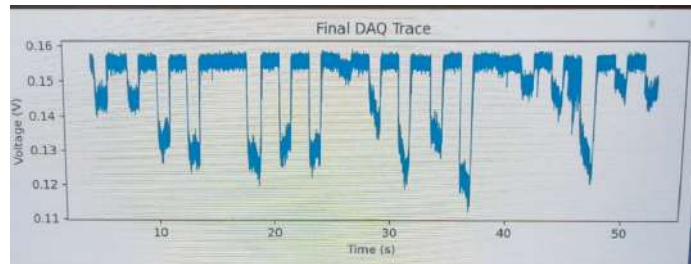
(3s / 2s lock / free-running cycle)

**Purchasing a More Expensive Controller Is Not a Solution**

The instability originates from control-path mismatch and output noise, not from insufficient controller performance. Replacing the controller with a higher-end unit would not resolve the system-level failure mode and would obscure, rather than fix, the underlying dynamics.

## 3. Custom Summing and Filtering Architecture

SC 110 Output Error - Solution 1: Voltage Divider+Noise Filtering

The SC 110 output range is 150 V, while PZT control requires only 65 V

- Soldered a voltage divider using 50-kΩ resistors
- **Impedance matching**
- This not only proportionally reduced the voltage error to **1.2 mV**, but also acted as a low pass filter, which further reduced the sharp peaks of transmission, as shown in the pictures.
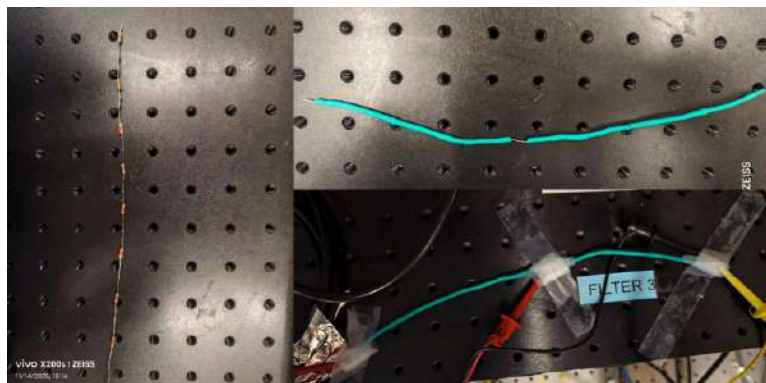
Voltage Divider and Filtering Result

Final DAQ Trace
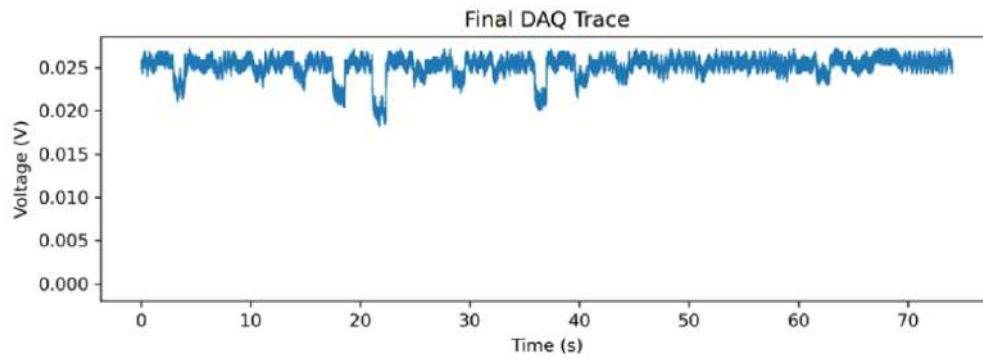
SC 110 Output Error - Solution 2: Inverting Summing Amplifier

I notice that the Digilock **Main Out** port does not suffer from the same DC offset error as the SC110. To exploit this, I build an **inverting summing amplifier** that combines:

Using a summing amplifier to add SC110 output with Main out, SC110 provide offset and Main out provides feedback to the cavity PZTs.

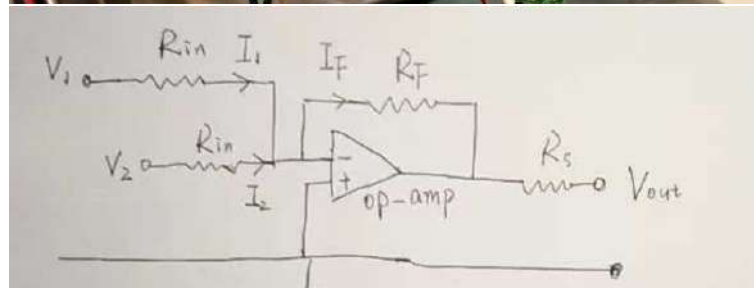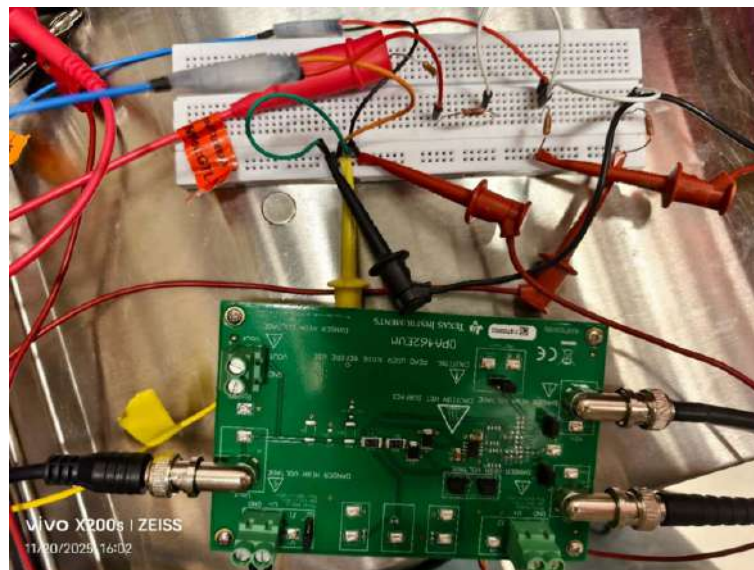High-Voltage Inverting Summing Amplifier (OPA462) + Voltage Divider

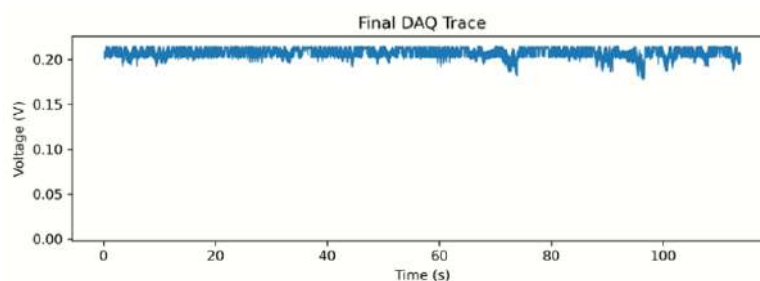$$R_F = R_{\text{in}} = 47.5k\Omega, \qquad R_s = 49.9k\Omega$$

$$I_1 = \frac{V_1}{R_{\text{in}}}, \qquad I_2 = \frac{V_2}{R_{\text{in}}}.$$

$$V_{\text{out}} = -R_F \left(\frac{V_1}{R_{\text{in}}} + \frac{V_2}{R_{\text{in}}} \right)$$

$$V_{\text{out}} = -(V_1 + V_2)$$

Results:

Final DAQ Trace

Quantified the resulting RMS noise.

SC110_sum_amp_AI3 Time-Domain Noise (DAQ)
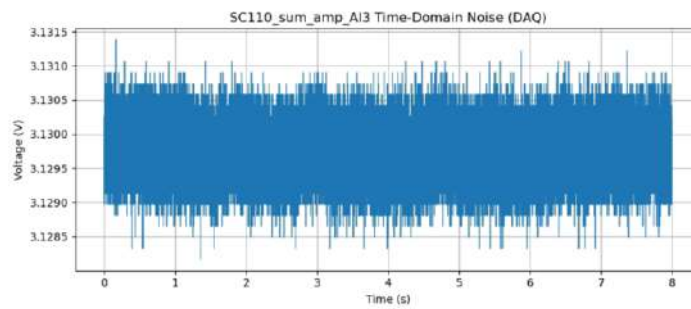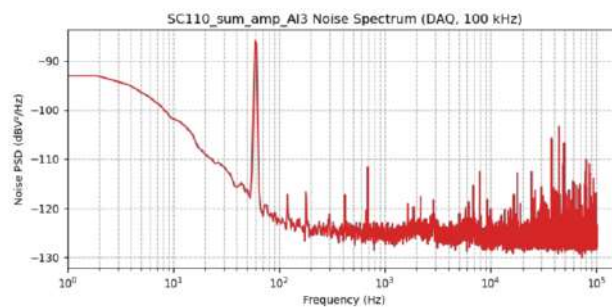
Figure 32

SC110_sum_amp_AI3 Noise Spectrum (DAQ, 100 kHz)

- **Noise RMS within 100KHz is 208.68uV**.
- Stable transmission during **lock 1s+free running 4mins cycles**
- Reliable cycling between **1-second lock and 4-minute unlock phases**.

Conclusion and Implications

I demonstrate that robust dynamic laser cleaning for microwave-to-optical transduction cannot be achieved through feedback tuning alone. Instead, it requires co-design of **control logic, actuation precision, and hardware interfaces**.

By reframing laser cleaning as a **state-dependent control problem**, I identify that lock failure originates from high-voltage output noise and control-path mismatch, not PID limitations. I then develop a timing-aware software framework and integrate custom analog filtering to enable repeatable lock-unlock cycles with stable free-running transmission.

The resulting system supports **fully automated laser cleaning** with millivolt-level actuation stability, reducing experimental overhead from tens of minutes to under one minute. More broadly, this work shows that **dynamic stability in quantum photonic systems emerges from integrated hardware-software design**, not from black-box controllers. In such experiments, the control system must be treated as an intrinsic part of the physical system.